IEICE TRANS. ELECTRON., VOL.E104–C, NO.4 APRIL 2021

BRIEF PAPER

Noise-Robust Distorted Born Iterative Method with Prior Estimate for Microwave Ablation Monitoring

Yuriko TAKAISHI[†], *Nonmember and* **Shouhei KIDERA**[†a)], *Member*

SUMMARY A noise-robust and accuracy-enhanced microwave imaging algorithm is presented for microwave ablation monitoring of cancer treatment. The ablation impact of dielectric change can be assessed by microwave inverse scattering analysis, where the dimension and dielectric drop of the ablation zone enable safe ablation monitoring. We focus on the distorted Born iterative method (DBIM), which is applicable to highly heterogeneous and contrasted dielectric profiles. As the reconstruction accuracy and convergence speed of DBIM depend largely on the initial estimate of the dielectric profile or noise level, this study exploits a prior estimate of the DBIM for the pre-ablation state to accelerate the convergence speed and introduces the matched-filter-based noise reduction scheme in the DBIM framework. The two-dimensional finite-difference time-domain numerical test with realistic breast phantoms shows that our method significantly enhances the reconstruction accuracy with a lower computational cost.

key words: *microwave ablation monitoring, microwave imaging, distorted born iterative method (DBIM), noise reduction*

1. Introduction

There is much research that supports the effectiveness of microwave ablation (MWA), which offers a minimally invasive, high-speed treatment by delivering thermal damage to cancerous tissues [1], including a number of clinical investigations into its impact on liver tumors [2] and other cancers such as those located in the kidney or breast. To avoid serious damage to normal tissues during ablation, a real-time and accurate monitoring modality is required for MWA treatment. Although various imaging modalities have been developed for this purpose, such as magnetic resonance imaging (MRI) [3] and ultrasound imaging, the MRI is unable to achieve real-time monitoring, and ultrasound imaging suffers from clutter responses because of heated microbubbles [4].

The microwave monitoring tool is regarded as one of the most promising alternatives to MRI and ultrasound imaging. It can overcome the above limitations and has numerous advantages in terms of compactness and compatibility with MWA treatment tools [7], where the dimensional evolution of the ablation zone can be characterized by examining the change of forward-scattered signals from the MWA probe to the external receivers. Some studies [5], [6] have demonstrated significant drops in dielectric properties after the ablation because of tissue hydration or thermal changes, thus requiring quantitative imaging for complex permittivity such as the distorted Born iterative method (DBIM) [8], which requires less assumptions, such as homogeneity or uniform dielectric drops in ablation zone Some real-time ablation zone estimators that exploit the signal difference between the pre-ablation and during ablation periods have been developed [9], [10], but these estimators require prior knowledge of the dielectric drop from the pre-ablation state and suffer from inaccuracy due to homogeneous assumptions or too much simplified propagation model. To avoid the above limitation, G. Chen *et al* introduced a tomographic approach using time-differential scattered data [11]. However, the reconstruction accuracy largely depends on the initial estimate of the dielectric map [8] and if it is not possible to obtain accurate prior knowledge of the dielectric profile, *i.e.*, the spatial distribution of the complex permittivity of the breast at the pre-ablation state, the approach would suffer from a sluggish convergence and would be insufficiently accurate. In real terms, the ablation zone image should be updated within a minute, which is a challenge for the tomographic approaches because it requires an iterative use of a forward solver, such as the finite-difference time-domain (FDTD) method.

To alleviate the above problem of dependency on the initial estimate and the computational cost, this study introduces a novel scheme for ablation zone monitoring by exploiting the feature of the DBIM that requires an initial background medium, *i.e.*, an dielectric profile assumed in the initial iteration step in the DBIM sequences, which is similar in both pre-ablation and during ablation states. However, since it is still impractical to obtain an accurate dielectric profile of the pre-ablation state as a prior knowledge, the proposed method firstly reconstructs the pre-ablation state with the original DBIM, where the initial estimate is set to the homogeneous media with an average complex permittivity of the breast. And then, the during ablation profile is sequentially updated by regarding the pre-ablation state as an updated background medium in the DBIM scheme. Furthermore, this study introduces matched-filter-based noise reduction in the DBIM framework, where its cost function is appropriately updated without a loss of computational efficiency. The two-dimensional (2-D) FDTD-based numerical investigations, assuming the MRI-derived realistic phantom, demonstrate that our proposed method considerably

Manuscript received May 21, 2020.
Manuscript revised August 24, 2020.
Manuscript publicized October 6, 2020.
[†]The authors are with Graduate School of Informatics and Engineering, The University of Electro-Communications, Chofu-shi, 182–8585 Japan.
a) E-mail: kidera@uec.ac.jp
DOI: 10.1587/transele.2020ECS6014

enhances the reconstruction accuracy and the noise robustness in the DBIM-based quantitative monitoring of the dielectric change of the ablation zone.

2. Method

We assume a typical microwave monitoring observation model, where multiple transmitters and receivers are configured at the external area of the object and $E^{\mathrm{t}}(\boldsymbol{r}_{\mathrm{t}}, \boldsymbol{r}_{\mathrm{r}}; t)$ is the total electric field at time t, with $\boldsymbol{r}_{\mathrm{t}}$ and $\boldsymbol{r}_{\mathrm{r}}$ being the positions of the transmitter and receiver, respectively.

2.1 Distorted Born Iterative Method (DBIM)

The forward problem in the electromagnetic scattering phenomena is formulated by solving the Helmholtz-type integral equation as:

$$\begin{aligned} E^{\mathrm{s}}(\boldsymbol{r}, \omega) &\equiv E^{\mathrm{t}}(\boldsymbol{r}, \omega) - E^{\mathrm{i}}(\boldsymbol{r}, \omega) \\ &= \omega^2 \mu \int_V G_{\mathrm{b}}(\boldsymbol{r}, \boldsymbol{r}', \omega) E^{\mathrm{t}}(\boldsymbol{r}', \omega) o(\boldsymbol{r}', \omega) \mathrm{d}\boldsymbol{r}', \quad (1) \end{aligned}$$

where ω denotes the angular frequency, $E^{\mathrm{t}}(\boldsymbol{r}, \omega)$ and $E^{\mathrm{i}}(\boldsymbol{r}, \omega)$ are the total electric fields with and without the presence of object, respectively. Ω denotes the region of interest (ROI) area, and $o(\boldsymbol{r}, \omega) \equiv \epsilon(\boldsymbol{r}, \omega) - \epsilon_{\mathrm{b}}(\boldsymbol{r}, \omega)$ is an object function, where $\epsilon_{\mathrm{b}}(\boldsymbol{r}, \omega)$ and $G_{\mathrm{b}}(\boldsymbol{r}, \boldsymbol{r}', \omega)$ denote the complex permittivity and the Green's function of the background media, respectively.

Under the Born approximation, Eq. (1) is expressed as:

$$\begin{aligned} \Delta E(\boldsymbol{r}, \omega) &\equiv E^{\mathrm{t}}(\boldsymbol{r}, \omega) - E^{\mathrm{t}}_{\mathrm{b}}(\boldsymbol{r}, \omega) \\ &\simeq \omega^2 \mu \int_V G_{\mathrm{b}}(\boldsymbol{r}, \boldsymbol{r}', \omega) E^{\mathrm{t}}_{\mathrm{b}}(\boldsymbol{r}', \omega) \Delta o(\boldsymbol{r}', \omega) \mathrm{d}\boldsymbol{r}, \quad (2) \end{aligned}$$

where $\Delta o(\boldsymbol{r}, \omega) \equiv o(\boldsymbol{r}, \omega) - o_{\mathrm{b}}(\boldsymbol{r}, \omega)$. To address a higher contrast case, the DBIM recursively updates the background media, the Green's function and its total field, denoted as $o_{\mathrm{b}}(\boldsymbol{r}, \omega)$, $G_{\mathrm{b}}(\boldsymbol{r}, \boldsymbol{r}', \omega)$ and $E^{\mathrm{t}}_{\mathrm{b}}(\boldsymbol{r}, \omega)$, respectively, so that $|\Delta E(\boldsymbol{r}, \omega)|^2$ takes a minimum. Numerous studies have shown that, although the DBIM produces an accurate target profile even in highly heterogeneous biological media, there is still an inherent problem in that it requires an appropriate initial estimate to achieve accurate and high-speed imaging.

2.2 DBIM with Prior Estimate and Matched Filtering

2.2.1 Principle

This study introduces a promising approach to address the above initial estimate dependency using the pre-ablation DBIM result. First, the DBIM without prior knowledge (*e.g.*, homogeneous media with average complex permittivity) is applied to the observation data at the pre-ablation state, and its reconstructed object function, Green's function and total field are defined as $\hat{o}^{\mathrm{pre}}_{\mathrm{b}}(\boldsymbol{r}, \omega)$, $G^{\mathrm{pre}}_{\mathrm{b}}(\boldsymbol{r}, \boldsymbol{r}', \omega)$ and $E^{\mathrm{t,pre}}_{\mathrm{b}}(\boldsymbol{r}, \omega)$, respectively. Then, the dielectric profile at the during ablation state is determined using the following cost function:

$$\begin{aligned} &\Delta \tilde{E}^{\mathrm{t}}(\boldsymbol{r}, \omega) = \\ &\omega^2 \mu \int_V G^{\mathrm{pre}}_{\mathrm{b}}(\boldsymbol{r}, \boldsymbol{r}', \omega) E^{\mathrm{t,pre}}_{\mathrm{b}}(\boldsymbol{r}', \omega) \Delta o^{\mathrm{pre}}(\boldsymbol{r}', \omega) \mathrm{d}\boldsymbol{r}', \quad (3) \end{aligned}$$

where $\Delta o^{\mathrm{pre}}(\boldsymbol{r}, \omega) = o(\boldsymbol{r}, \omega) - \hat{o}^{\mathrm{pre}}(\boldsymbol{r}, \omega)$. The reconstructed result is denoted as $\hat{o}^{\mathrm{dur}}(\boldsymbol{r}, \omega)$. The dielectric profile of the ablation zone is determined as:

$$\Delta \hat{o}(\boldsymbol{r}, \omega) = \hat{o}^{\mathrm{dur}}(\boldsymbol{r}, \omega) - \hat{o}^{\mathrm{pre}}(\boldsymbol{r}, \omega), \quad (4)$$

Note that, the reconstruction accuracy of the DBIM significantly depends on the selection of the initial background media, because it is based on the optimization scheme. Then, an appropriate initial estimate of the background media could enhance the reconstruction accuracy with much fewer iteration steps. Since the dielectric profile at the pre-ablation state $o^{\mathrm{pre}}(\boldsymbol{r}, \omega)$ is relatively similar to that at the during ablation state $o^{\mathrm{dur}}(\boldsymbol{r}, \omega)$, the DBIM requires far fewer iterations by replacing the background media as $o^{\mathrm{pre}}(\boldsymbol{r}, \omega)$.

Furthermore, for a noise-reduction purpose, the matched filter process is introduced for the cost function of the DBIM. It is well known that the matched filter (cross-correlation process in the time-domain) is the most noise-robust filter and the cost function is then, modified as:

$$\Delta E^{\mathrm{match}}(\boldsymbol{r}, \omega) = \Delta \tilde{E}^{\mathrm{t}}(\boldsymbol{r}, \omega) E^{*}_{\mathrm{ref}}(\omega) \quad (5)$$

where $*$ denotes the complex conjugate and $E_{\mathrm{ref}}(\omega)$ denotes the frequency response of the reference signal, which is usually observed as a transmitting signal in free-space.

2.2.2 Procedure

Figure 1 shows the schematic diagram of the proposed method, which is detailed as follows:

Step 1) The dielectric profile at the pre-ablation state is reconstructed by the DBIM as $\hat{o}^{\mathrm{pre}}(\boldsymbol{r}, \omega)$ with the matched filtered cost function in Eq. (5), where the initial map $o^{\mathrm{init}}(\boldsymbol{r}, \omega)$ is given as $o_{\mathrm{b}}(\boldsymbol{r}, \omega)$ by homogeneous media with the average complex permittivity of the breast tissue.

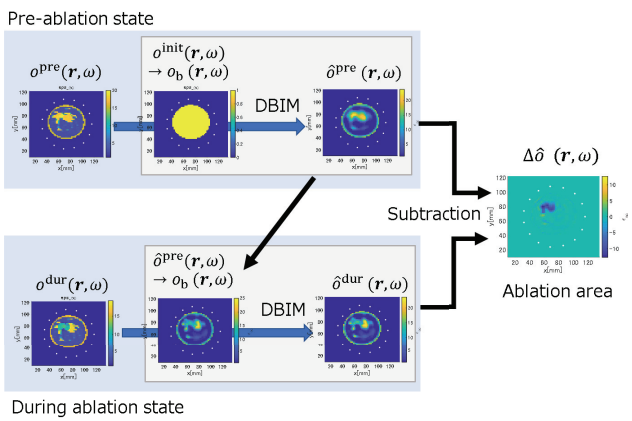

Fig. 1 Schematic diagram of the proposed method, where a prior profile in pre-ablation state is provided by the original DBIM.

Step 2) The dielectric profile at the during-ablation state is reconstructed by the DBIM as $\hat{o}^{\mathrm{dur}}(\boldsymbol{r}, \omega)$ with the matched filtered cost function in Eq. (5), where the initial map is given by $\hat{o}^{\mathrm{pre}}(\boldsymbol{r}, \omega)$, that is, Eq. (3).

Step 3) The permittivity profile of the ablation zone $\Delta\hat{o}(\boldsymbol{r}, \omega)$ is determined in Eq. (4).

3. Numerical Tests

3.1 Breast Phantom and Measurement Array

The numerical test, using the 2-D FDTD analysis of in-house University of Wisconsin-Madison codes, is investigated using the MRI-derived realistic numerical phantom of the breast, a Class-3 "heterogeneously dense" phantom (ID number 062204), which is available from [12]. The frequency dependency for each breast tissue is modeled by single-pole Debye models as

$$\epsilon(\omega) = \epsilon_\infty + \frac{\Delta\epsilon}{1 + j\omega\tau_0} + \frac{\sigma}{j\omega\epsilon_0}, \tag{6}$$

using a frequency range of 0.1 to 5.0 GHz [13]. Figure 2 shows the map of $\Delta\epsilon$ of the Class-3 breast phantom and the observation geometry. The transmitted current is excited inside the breast tissue, which should be within the fibroglandular tissue, including the 2 mm radius circular-shape cancer with $(\epsilon_\infty, \Delta\epsilon, \sigma) = (58.0, 20.0, 0.8\mathrm{S/m})$. The 15 receivers, which are situated in the air with equal spacing, circle the breast tissues. The transmitted current has a pulse with a center frequency of 2.45 GHz and a bandwidth of 1.9 GHz. The cell size for the FDTD and the unknown pixel in the DBIM is set to 2 mm. We assume that all Debye parameters uniformly drop in the ablation zone, indicating that the inside and outside dielectric properties have a heterogeneous map. The ratio between the pre-ablation and during ablation states of complex permittivity is denoted as ξ, and this simulation test the case, where the impact of the ablation is $\xi = 0.6$ is investigated, namely, the uniform 40 % drops in all Debye parameters in the ablation zone, which corresponds to an ablation of 99°C of the bovine liver tissues [5]. The ablation zone is modeled as ellipsoidal shape with 20 mm and 16 mm diameters along the x-axis and y-axis, respectively as in Fig. 2.

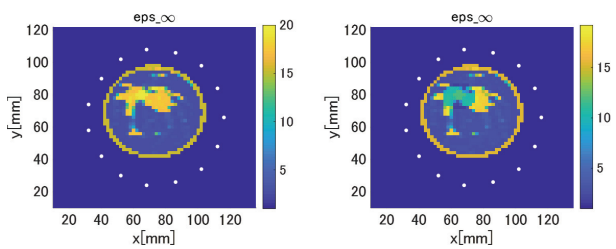

Fig. 2 Original profile of Debye parameter of ϵ_∞. (a) Pre-ablation state. (b) During ablation state.

3.2 Results: Effect of Prior Estimate of Pre-Ablation State

The results for validating the effectiveness of a prior estimate of the pre-ablation state, that is, the process described in Eq. (3), are discussed below. To eliminate the error caused by noise in the discussion, a noiseless situation is assumed. Figure 3 shows the difference of the DBIM reconstruction results between the during and pre-ablation state of each Debye parameter as ϵ_∞, $\Delta\epsilon$, and σ_s, which are representative forms of the differences of $\Delta\hat{o}(\mathbf{r}, \omega)$ in Eq. (4), in assuming the single-pole Debye model as in Eq. (6). Here, the number of iterations of DBIM is set to 10 in each case. Table 1 summarizes the quantitative error comparison as cumulative probabilities for each error criteria. Here, the error values $\mathrm{Err}_{\epsilon_\infty}$, $\mathrm{Err}_{\Delta\epsilon}$, and Err_{σ_s} denote the difference between the true and estimated values of ϵ_∞, $\Delta\epsilon$, and σ_s, respectively, at each position of the ROI. As shown in these figures and in Table 1, the DBIM reconstruction without prior knowledge of pre-ablation results suffers from considerably inaccuracy, and hardly estimates the actual dimension of ablation zone. A reconstruction using pre-ablation prior knowledge, however, creates a more accurate ablation zone area, including its quantitative dielectric drop. The computational times for estimating the pre-ablation state are within 60 s for both cases with or without using the matched filtering process, which is an acceptable duration because a general temporal evolution of the ablation zone occurs in a minute scale [5].

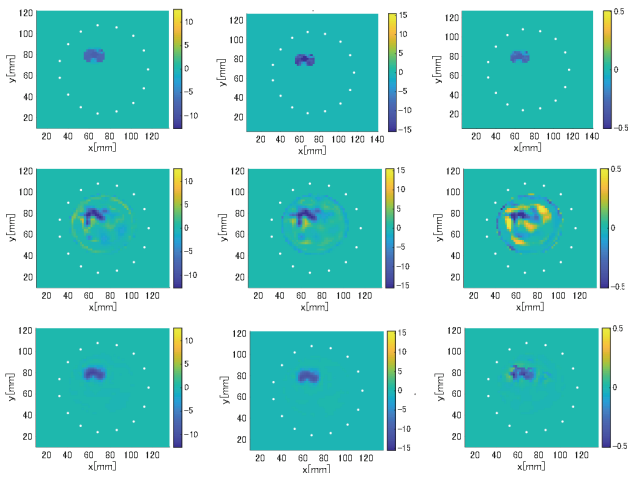

Fig. 3 Reconstruction results of difference maps between pre- and during ablation state for each Debye parameter by DBIM based methods at noiseless case. First line: original. Second line: DBIM w/o prior estimate. Third line :DBIM w prior estimate. First column: ϵ_∞. Second column : $\Delta\epsilon$. Third column : σ.

Table 1 Cumulative probability w or w/o prior estimate, where the iteration number is 10 in noiseless case.

	$\mathrm{Err}_{\epsilon_\infty} \le 2$	$\mathrm{Err}_{\Delta\epsilon} \le 2$	$\mathrm{Err}_{\sigma_s} \le 0.1$
w/o prior estimate	77.1 %	71.0 %	62.0 %
w prior estimate	95.2%	92.9 %	92.4 %

3.3 Results: Effect of Matched Filter Noise Reduction

Next, we show the noise-robust feature of the matched-filter-based noise reduction described in Eq. (5). Here, we use the reference signal of the matched filter as the direct propagation signal from the source to the receiver in a free-space, where we have confirmed that this waveform is not so much different from the forward scattering signal propagating into the breast media. An additive white Gaussian additive noise is directly added to each received signal in the time domain, the relevance of which has been validated in the number of studies [7], [10]. The signal-to-noise ratio (SNR) is defined as the ratio of the maximum power of the received signals to the power of noise in the time domain. As a representative lower SNR case, 10 dB SNR is investigated, which is regarded as quite lower SNR case denoted in [9]. Figure 4 shows the results obtained by each process, including those with and without matched filtering. In addition, Tables 2 and 3 show the quantitative error comparison for cases with and without pre-ablation prior estimates. As shown in the results, the matched-filter-based reconstruction produces the most robust reconstruction performance with appropriate ablation dimensions even in the lower SNR case.

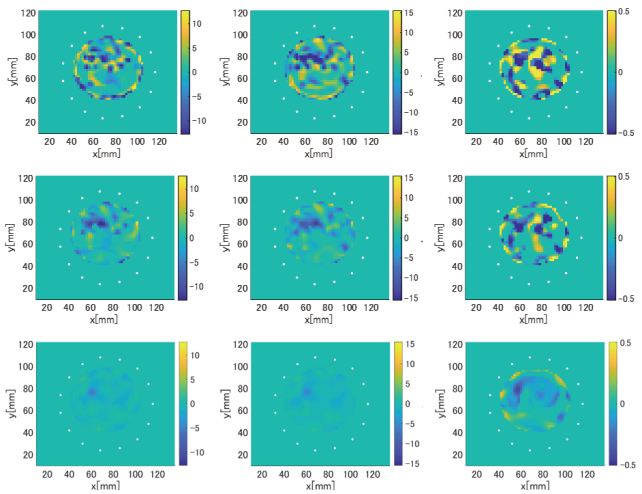

Fig. 4 Reconstruction results of difference maps between pre- and during ablation state for each Debye parameter by DBIM based methods at SNR = 10 dB. First line: DBIM w/o prior estimate and matched filtering. Second line: DBIM w prior estimate but w/o matched filter. Third line: DBIM w prior estimate and matched filter. First column: ϵ_∞. Second column: $\Delta\epsilon$. Third column: σ.

Table 2 Cumulative probability comparison for w and w/o matched filter at 10 dB SNR for the case w/o prior estimate.

w/o prior estimate	$\mathrm{Err}_{\epsilon_\infty} \leq 2$	$\mathrm{Err}_{\Delta\epsilon} \leq 2$	$\mathrm{Err}_{\sigma_s} \leq 0.1$
w/o matched filter	44.4%	30.1%	43.5%
w matched filter	49.9%	42.2%	40.8%

Table 3 Cumulative probability comparison for w and w/o matched filter at 10 dB SNR for the case w prior estimate.

w prior estimate	$\mathrm{Err}_{\epsilon_\infty} \leq 2$	$\mathrm{Err}_{\Delta\epsilon} \leq 2$	$\mathrm{Err}_{\sigma_s} \leq 0.1$
w/o matched filter	64.8%	56.7%	52.5%
w matched filter	92.2%	92.0%	66.9%

4. Conclusion

This study introduced a noise-robust and accurate ablation zone monitoring algorithm based on a prior DBIM quantitative reconstruction scheme. In the proposed method, the pre-ablation reconstruction is introduced as an initial estimate of DBIM for the during ablation state to enhance the convergence speed and reconstruction accuracy. Furthermore, we implemented the DBIM cost function to matched filter processing for a more noise-robust estimate. The 2-D FDTD numerical analysis with the MRI-derived phantom demonstrated that our approach showed a notable improvement in reconstruction accuracy with a relevant reconstruction speed, which maintains its performance even in a quite-low-SNR scenario. Note that, the reconstruction accuracy of the proposed method significantly depends the initial estimate of the pre-ablation state. To address the above concerns, the hybrid use of the other methods, like [10] are promising, by adding an independent *a priori* information of ablation zone. A three-dimensional expansion and experimental validation should be pursued further in the future.

Acknowledgments

This research and development work were supported by the MIC/SCOPE # 162103102.

References

[1] G. Carrafiello, D. Lagana, M. Mangini, F. Fontana, G. Dionigi, L. Boni, F. Rovera, S. Cuffari, and C. Fugazzola, "Microwave tumors ablation: Principles, clinical applications and review of preliminary experiences," Int. J. Surg., vol.6, Supplement 1, pp.S65–S69, Dec. 2008.

[2] R.C.G. Martin, C.R. Scoggins, and K.M. McMasters, "Safety and efficacy of microwave ablation of hepatic tumors: a prospective review of a 5-year experience," Ann. Surg. Oncol., vol.17, no.1, pp.171–178, Jan. 2010.

[3] L.G. Merckel, L.W. Bartels, and M.O. Kohler, H.J.G.D. van den Bongard, R. Deckers, W. Mali, C. Binkert, C.T. Moonen, K.G.A. Gilhuijs, and M.A.A.J. van den Bosch, "MR-guided high-intensity focused ultrasound ablation of breast cancer with a dedicated breast platform," Cardiovasc. Intervent. Radiol., vol.36, no.2, pp.292–301. April 2013.

[4] M.D. Correa-Gallego, A.M. Karkar, and S. Monette, P.C. Ezell, W.R. Jarnagin, and T.P. Kingham, "Intraoperative ultrasound and tissue elastography measurements do not predict the size of hepatic microwave ablations," Acad. Radiol., vol.21, no.1. pp.72–78, Jan. 2014.

[5] V. Lopresto, R. Pinto, G. A Lovisolo, and M. Cavagnaro, "Changes in the dielectric properties of ex vivo bovine liver during microwave thermal ablation at 2.45 GHz," Phys. Med. Biol. vol.57, no.8, pp.2309–2327, 2012.

[6] R.O. Mays, N. Behdad, and S.C. Hagness, "Array Sensitivity for Model-Based Microwave Breast Imaging," IEEE Trans. Antennas Propag., vol.65, no.6, pp.100, June 2017.

[7] O.M. Bucci, M. Cavagnaro, L. Crocco, V. Lopresto, and R. Scapaticci, "Microwave Ablation Monitoring via Microwave Tomography: a Numerical Feasibility Assessment," Proc. 2016 10th European Conference on Antennas and Propagation, 2016.

[8] F. Gao, B.D. Van Veen, and S.C. Hagness, "Sensitivity of the distorted Born iterative method to the initial guess in microwave breast imaging," IEEE Trans. Antennas Propag., vol.63, no.8, pp.3540–3547, Aug. 2015.

[9] S. Kidera, L.M. Neira, B.D. Van Veen, and S.C. Hagness, "TDOA-based microwave imaging algorithm for real-time microwave ablation monitoring," Int. J. Microwave and Wireless Technologies, vol.10, no.2, pp.169–178, March 2018.

[10] K. Kanazawa, K. Noritake, Y. Takaishi, and S. Kidera, "Microwave Imaging Algorithm Based on Waveform Reconstruction for Microwave Ablation Treatment," IEEE Trans. Antennas Propag., pp.5613–5625, vol.68, no.7, July 2020.

[11] G. Chen, J. Stang, M. Haynes, E. Leuthardt, and M. Moghaddam, "Real-Time Three-Dimensional Microwave Monitoring of Interstitial Thermal Therapy," IEEE Trans. Biomedical Engineering, vol.65, no.3, pp.528–538, March , 2018.

[12] University of Wisconsin Cross-Disciplinary Electromagnetics Laboratory (UWCEM), "Numerical breast phantom repository," [Online]. Available: http://uwcem.ece.wisc.edu, accessed on: Oct. 2, 2017.

[13] M. Lazebnik, D. Popovic, L. McCartney, C.B Watkins, M.J Lindstrom, J. Harter, S. Sewall, T. Ogilvie, A. Magliocco, T.M Breslin, W. Temple, D. Mew, J.H Booske, M. Okoniewski, and S.C Hagness, "A large-scale study of the ultrawideband microwave dielectric properties of normal, benign, and malignant breast tissues obtained from cancer surgeries," Physics in Medicine and Biology, vol.52, pp.6093–6115, 2007.